19th Brazilian Congress of Thermal Sciences and Engineering
November 06th-10th, 2022, Bento Gonçalves - RS - Brazil

ENC-2022-0357
NUMERICAL MODELING OF THE THERMAL PERFORMANCE OF A HYBRID SOLAR INVERTER

Otavio Duarte Aires Heckler
Programa de Pós-Graduação em Engenharia Oceânica - PPGEO, Universidade Federal de Rio Grande – FURG, Italy Avenue, km 8, CEP 96203- 900, Rio Grande, RS, Brazil.
otaviooduarte@gmail.com

Rafael Christiano Annunziato
NHS SISTEMAS ELETRÔNICOS LTDA, Av. Juscelino Kubitscheck de Oliveira, n.º 5270, Curitiba, PR, Brazil.
rafael@nhs.com.br

Welington Fernando Lima Desan
RADEK SISTEMAS DE INFORMAÇÃO LTDA Avenida República Argentina, nº 2275, Curitiba, PR, Brazil.
wdesan@radek.com.br

Marcus Vinicius Alves Pereira
Programa de Pós Graduação em Engenharia Mecânica – PGMEC, Universidade Federal do Paraná – UFPR, CEP 81531-980, Curitiba, PR, Brazil.
marcusvap15@gmail.com

Jeferson Avila Souza
Programa de Pós-Graduação em Engenharia Oceânica - PPGEO, Universidade Federal de Rio Grande – FURG, Italy Avenue, km 8, CEP 96203- 900, Rio Grande, RS, Brazil.
jasouza@furg.br

Abstract. *The increasing usage of electronic devices have improved performance and capabilities of most domestic and industrial equipment. In many applications, they are becoming smaller, more powerful and assembled inside a cabinet with limited volume size. Thermal management of such products is crucial to guarantee high performance under normal operating conditions. Present work numerically investigates the thermal behavior of a hybrid solar inverter subjected to natural convection cooling. Main objective is to calculate temperature gradients inside the cabinet and guarantee that maximum equipment temperature remains below critical values. The solution accounts for a close to real equipment geometry, including the cabinet, circuit board and heat sink (fins) and the major heat sources: IGBTs and inductor. A Finite Volume numerical solution is obtained with the OpenFOAM software, more specifically using the chtMultiRegionFoam solver, while geometry discretization was performed with the snappyHexMesh utility (also included with OpenFOAM software). The model assumes an incompressible flow with constant thermophysical properties and uses the Boussinesq approximation to model the natural convection. Energy equation is solved for both solid and fluid regions. Temperature and velocity profiles, inside the inverter cabinet, were calculated and their influence to the thermal management of the overall system is analyzed. Equipment temperatures (maximum and average) are also investigated for steady state conditions. Results have allowed to identify the domain regions with higher temperatures and/or flow stagnation. These locations indicate the regions where natural convection is ineffective and the positions where the equipment with higher energy dissipation should not be positioned.*

Keywords: *Natural convection, Thermal management, Open source, Finite volume solution*

1. INTRODUCTION

Photovoltaic (PV) inverters are equipment used to convert from DC to AC the generated electrical energy. The built-in electronic equipment dissipate a considerable among of energy, which must be removed to guarantee the safe system operation. If this heat is not removed, system temperature will increase and the inverter performance will be

affected. Moreover, the power output is reduced with the increase of the system temperature (Jeykishan Kumar et al., (2021)).

Due to its importance, there are many models to predict the performance of PV systems. In most of them, as can be observed in the work of Roberts et al., (2017), which studied 20 PV performance models, temperature is one of the most important parameters to be taken into account. Specifically about the inverter, the importance and difficult of predicting the thermal behavior is discussed in the work of Rampinelli et al., (2017). In their work, it is proposed a methodology to analyze the inverter thermal behavior, however to improve the model predictions, two experimental coefficients need to be evaluated. Another example of thermal modeling is presented by Figueiredo et al., (2021), on which an empirical model is used to determine the inverter losses due to power limitations imposed by the temperature. These two examples use mathematical models to describe the system dynamics in terms of empirical parameters and do not solve the fluid flow heat exchange problem inside the inverter.

In present work, thermal performance of a photovoltaic inverter is investigated with a CFD (Computational Fluid Dynamics) solution. All important equipment are considered in the study and the discretized domain geometry is very close to the real one. System cooling is obtained with natural convection and 8 different conditions were investigated. Results have shown that depending on the number of heat sources (IGBTs), the system temperature may reach temperature values above the recommended.

2. PROBLEM DESCRIPTION

The simplified geometry of a photovoltaic hybrid inverter is show in Fig. 1. It contains the most important equipment with most of the details. Shown equipment presented in Fig. 1 are: circuit board, fins, inductor and IGBTs. There are five heat sources that can be on simultaneous or not, resulting in different thermal conditions and different cooling down requirements. The inductor is always on and dissipates 18 W, while the IGBTs dissipate 70 W each, but are not always on. The inverter has two cabinets: a superior one containing the circuit board and an inferior one containing the inductor, the IGBTs and the fins. They are separated by an internal wall not show in Fig. 1.

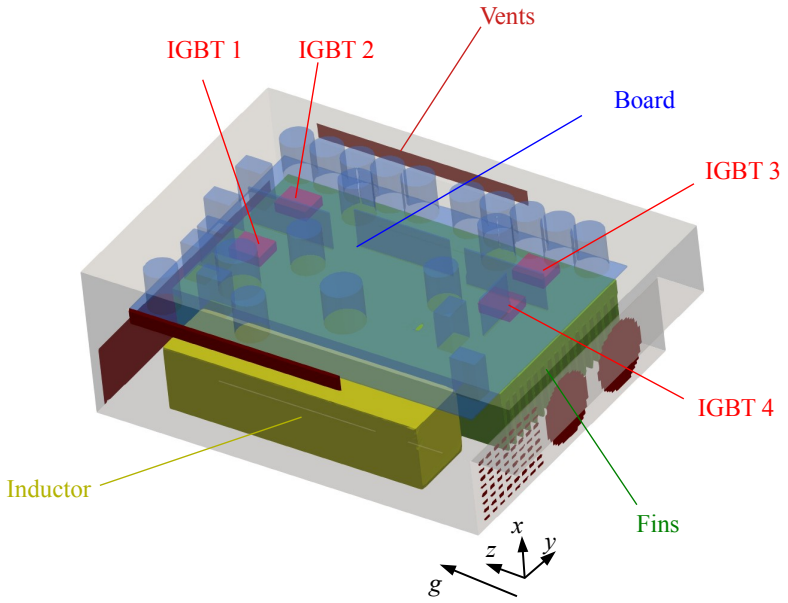

Figure 1. Computational domain.

2.1. Flow Modeling

Only natural convection is considered in this work. The flow is assumed incompressible and the Boussinesq approximation is used to model the buoyancy force (Bejan, (1993)). Turbulence is modeled with the Reynolds Average Navier-Stokes formulation using the κ-ε model (Versteeg and Malalasekra, (2007)). The time average continuity and momentum equations are given, respectively, by

$$\frac{\partial \bar{u}_i}{\partial x_i} = 0 \tag{1}$$

$$\rho\frac{\partial \bar{u}_i}{\partial t}+\rho\frac{\partial}{\partial x_j}\left(\bar{u}_j\bar{u}_i\right)=-\frac{\partial \bar{p}_i}{\partial x_i}+\frac{\partial}{\partial x_j}\left[\left(\mu+\mu_t\right)\left(\frac{\partial \bar{u}_i}{\partial x_j}+\frac{\partial \bar{u}_j}{\partial x_i}\right)-\frac{2}{3}\frac{\partial \bar{u}_k}{\partial x_k}\delta_{ij}\right]+\rho_0 g_i\left[1-\beta\left(T-T_\infty\right)\right] \tag{2}$$

where $\bar{u}$ is the time averaged velocity [m/s], t is the time [s], $\bar{p}$ is the time averaged pressure [Pa], x represents the Cartesian coordinates [m], g is the gravity acceleration [m/s²], μ the eddy viscosity [m²/s], ρ is the fluid density [kg/m³] and β the thermal expansion coefficient [1/K]. Indexes i, j and k = 1, 2, 3 corresponds to the x, y and z directions, respectively.

Coupling with the turbulence model is obtained by defining the turbulent eddy viscosity as

$$\mu_t=\rho C_\mu\frac{\kappa^2}{\varepsilon} \tag{3}$$

where μ_t is the turbulent eddy viscosity [m²/s], κ is the turbulent kinetic energy [m²/s²], ε the rate of viscous dissipation [m²/s³], and C_μ = 0,09 a model constant.

The κ-ε model is then closed with the addition of two transport equations: one for the turbulent kinetic energy

$$\frac{\partial}{\partial t}\left(\rho\varepsilon\right)+\frac{\partial}{\partial x_i}\left(\rho\bar{u}_i\varepsilon\right)=\frac{\partial}{\partial x_i}\left(\frac{\mu_t}{\sigma_\epsilon}\frac{\partial \varepsilon}{\partial x_i}\right)+C_{1\epsilon}\frac{\varepsilon}{\kappa}2\mu_t S_{ij}-C_{2\epsilon}\rho\frac{\varepsilon^2}{\kappa} \tag{4}$$

and a second equation for the viscous dissipation

$$\frac{\partial}{\partial t}\left(\rho\varepsilon\right)+\frac{\partial}{\partial x_i}\left(\rho\bar{u}_i\varepsilon\right)=\frac{\partial}{\partial x_i}\left(\frac{\mu_t}{\sigma_\epsilon}\frac{\partial \varepsilon}{\partial x_i}\right)+C_{1\epsilon}\frac{\varepsilon}{\kappa}2\mu_t S_{ij}-C_{2\epsilon}\rho\frac{\varepsilon^2}{\kappa} \tag{5}$$

where the model constants are: σ_κ = 1.00, σ_ε = 1.30, $C_{1\varepsilon}$ = 1.44 and $C_{2\varepsilon}$ = 1.92 and the mean rate of deformation S_{ij} [1/s], given by

$$S_{ij}=\frac{1}{2}\left(\frac{\partial \bar{u}_i}{\partial x_j}+\frac{\partial \bar{u}_j}{\partial x_i}\right) \tag{6}$$

The model is closed with the energy equation given by

$$\frac{\partial \bar{T}}{\partial t}+\frac{\partial}{\partial x_i}\left(\bar{u}_i\bar{T}\right)=\frac{\partial}{\partial x_i}\left[\left(\alpha+\alpha_t\right)\frac{\partial \bar{T}}{\partial x_i}\right] \tag{7}$$

where T is the temperature [K], α is the thermal diffusivity [m²/s] and α_t is the turbulent thermal diffusivity [m²/s].

At the beginning of the simulation, all fluid and solid surfaces are at 20 °C. Boundary conditions for the fluid flow problem are: prescribe zero (gauge) pressure at all vents and no slip at all other external and internal surfaces. For the rate of viscous dissipation, zero gradient (normal to the surface) was specified to all vents and a turbulence dissipation wall constraint was set to all solid boundaries. For the turbulent kinetic energy, zero gradient was set to all boundaries. For the thermal problem, zero gradient was specified at all vent sections. Two conditions were tested for the external cabinet walls: i) insulated and ii) convection with aluminum walls. It was also set the ambient air temperature T_∞ = 20 °C, the external walls thickness equal to 1 mm, the heat transfer coefficient h = 4,7 W/m² K and the thermal conductivity k_{aluminum} = 200 W/m K. The inverter is assumed to be indoor.

2.2. Numerical solution

Solution was obtained with a finite volume formulation (Versteeg and Malalasekra, (2007)) using the OpenFOAM software (Weller et al., n.d.). More specifically it was used the *chtMultRegionFoam* solver, which is the OpenFOAM implementation to solve multi-region (solid and fluid) thermal and fluid flow problems. Solution was controlled by limiting the Courant number to 1 and the diffusion number to 10. For all equations, upwind was used to discretize the divergent terms while a Gauss central difference scheme was used in the gradient schemes. Only steady state solution is analysed, thus a pseudo-transient scheme was used to integrate equations in time.

The solution independence with the grid was also investigated. The *snappyHexMesh* utility (part of the OpenFOAM distribution) was used to discretize the computational domain. Five grids were tested and the independent one has approximated 1,000,000 volumes. Most of the volumes are hexahedrons, however some tetrahedrons were created (~10%) due to the complexity of the geometry. A print of the independent grid is show in Fig. 2.

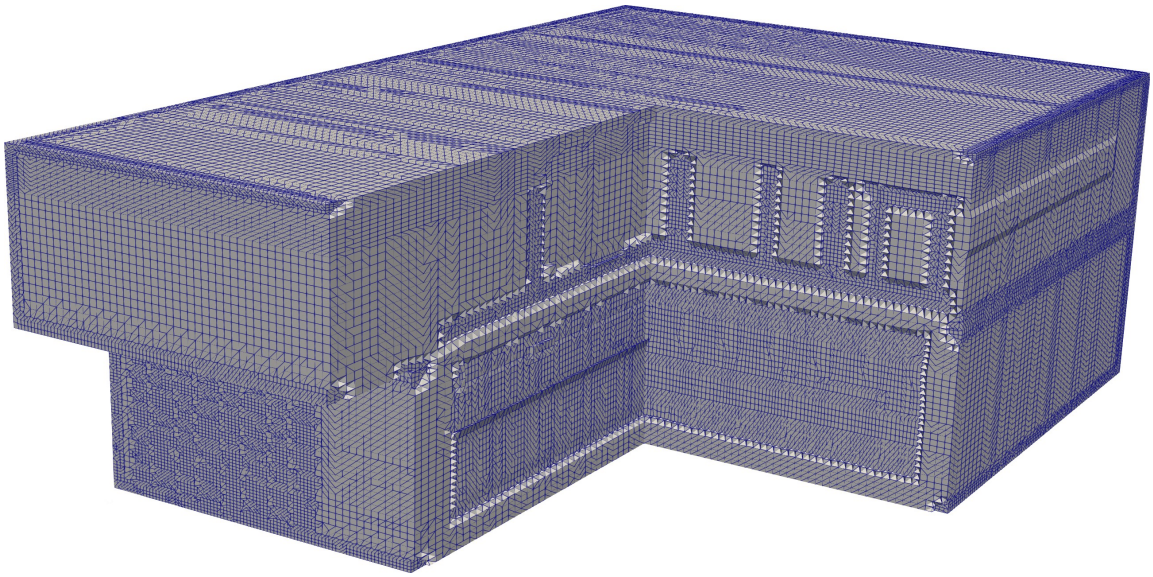

Figure 2. Independent grid.

3. RESULTS

For all simulations, temperature is monitored at the main equipment (circuit board, fins, inductor and IGBTs) and inside the inferior and superior cabinets. Main goal was to evaluate the average and maximum temperatures inside the inverter and determine the limiting loading conditions that can be cooled down with natural convection only.

Figure 3 presents maximum temperature results for all 8 performed simulations. Colors indicate the number of heat sources (IGBTs) that are on and continuous and dashed lines indicate the condition applied to the external walls: insulated and aluminum, respectively. For all power conditions, it can be observed from Fig. 3 that the maximum temperature inside the inverter does not vary to much (less than 10 °C) among the different equipment. It is higher at the IGBTs 1 and 2, which are positioned close to the superior vents (outlets) and lower at IGBTs 3 and 4 which are close to the inferior vents (inlets).

It is also possible to observe in Fig. 3 the influence of the cabinet walls material. These walls are ether manufactured with polymeric fibrous composite or metallic material, represented here as insulated or aluminum, respectively. The insulated walls are a limiting condition that represent the worst possible condition, however polymeric composites have low thermal conductive, making this choice a good approximation. Moreover, results presented in Fig. 3 show that the external walls condition have no great effect on maximum equipment temperatures. Maximum difference of approximated 5 °C was observed at IGBT 4, for the condition where all heat sources (green curve in Fig. 3) are on.

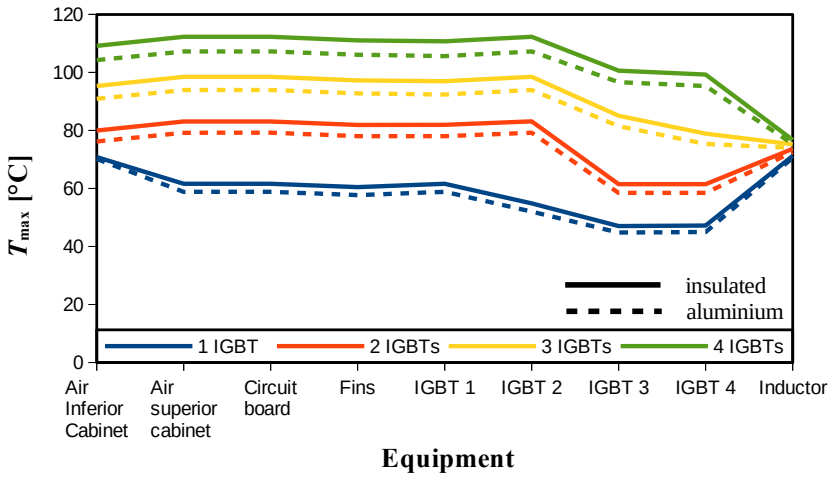

Figure 3. Main equipment and cabinets maximum temperatures.

The average temperature of all equipment and air cabinets were also evaluated and results are presented in Fig. 4. The major difference between profiles in Figs. 3 and 4 is for the air cabinet temperatures, which average values are considerably lower. This is due because for the air inside the cabinets, maximum temperature occurs next to the hot equipment, having a value close to it. Far from the equipment, air is moving at higher velocities and have lower temperature values.

In terms of the influence of the external walls materials, a temperature about 13 °C higher was calculated inside the air superior cabinet (the one containing the circuit board) for the insulated case and all four heat sources on. It is more than twice the increase in maximum temperature and a clear indication that a considerable larger amount of energy remains inside the inverter when walls are assumed insulated.

Another interesting result that can be obtained from Figs. 3 and 4 is that the inductor is almost not affected by the IGBTs power load. For all 4 load conditions, while all equipment maximum temperature increases from ~60 °C to more than 100 °C, the inductor maximum temperature increases only 5 °C. Similar behavior is also observed in Figs. 4, for the average temperature. This can be explained by observing in Fig. 1 the location of the inductor (in yellow). It is neither in contact with the IGBTs nor the heat sink (fins) and air flow can pass through it almost without getting in contact with any hot equipment.

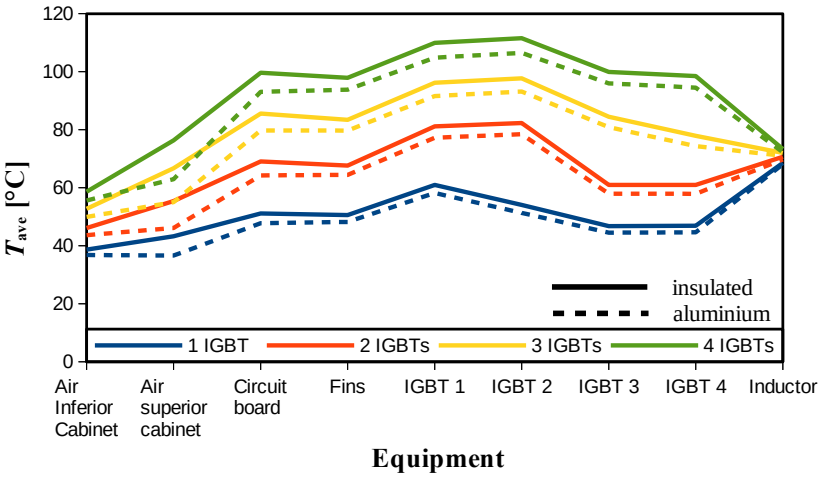

Figure 4. Main equipment and cabinets average temperatures.

Temperature fields for the circuit board are presented in Fig. 5 for all simulated cases. This is a top view which does not allow the visualization of the heat sources (IGBTs), however their positions are marked with dashed white lines.

As already commented in discussion of Figs. 3 and 4, temperature differences obtained for the insulated and aluminum external walls solutions are small. Thus, it is difficult to compare the temperature fields in Fig. 5. However, from the information of the maximum temperature, which is also presented in Fig. 5, it is possible to realize that solutions are not identical. Actually, it is possible to visualize small differences between the insulated and aluminum figures.

Once only natural convection is considered, flow moves against gravity acceleration, from cold to hot regions, i. e., against z direction in Fig. 5. Even at the lowest heat load condition, when only one IGBT is on, the whole circuit board reaches the steady state condition with a temperature approximately 20 °C above the inlet air temperature (20 °C). At this condition (IGBT 1 on), temperature gradients are small and a hot spot can be observed in the region where IGBT 1 is positioned. When IGBT 2 is turned on, whole circuit board temperature increases and a hot region is observed at the right superior region. Finally, IGBTs 3 and then 4 are turned on, resulting in similar temperature fields with higher temperatures at the right.

In terms of thermal management, simulation results showed that temperatures will significantly increase when the power load increases. For cases with 3 and 4 IGBTs on, temperatures above 90 °C were calculated. According to Tan et al., (2022), the IGBTs can operate with temperatures up to 170 °C, however the recommended operating temperature is about 80 °C. At high temperatures, the inverter will operate with lower power and some electronic equipment may be damaged. Assuming this limiting condition, the inverter studied in this work can only operates with two IGBTs simultaneous on. For higher load powers, it would be necessary to use forced convection by adding one or two fans to the system.

From Figs. 3 and 4 it can also be verified that if other heat dissipation equipment needed to be assembled in the circuit board, the bottom left corner would be the recommended location. Perhaps, repositioning of the IBGTs would also be an alternative to better distribute the generated heat, however this repositioning study can not be performed only

taking into account fluid flow and thermal analysis, thus it was decided not to change the IGBTs position.

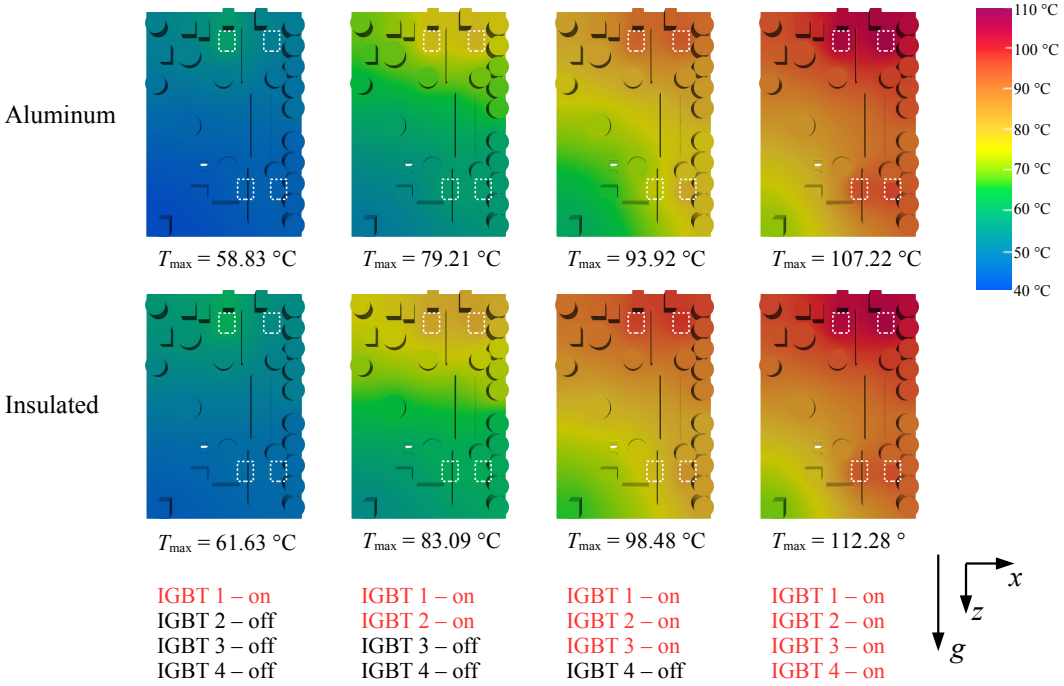

Figure 5. Temperature fields for the circuit board.

Temperature fields for the fins and the four IGBTs are presented in Fig. 6 for all studied cases. Likewise what has been discussed in relation to Fig. 5, temperature increases with the load and it is higher close to the top right corner. It can be seen in Fig. 6 that temperature distribution at the heat sink (fins) is more or less well distributed, i. e., all heat sink mass is heated and helps to cool down the system.

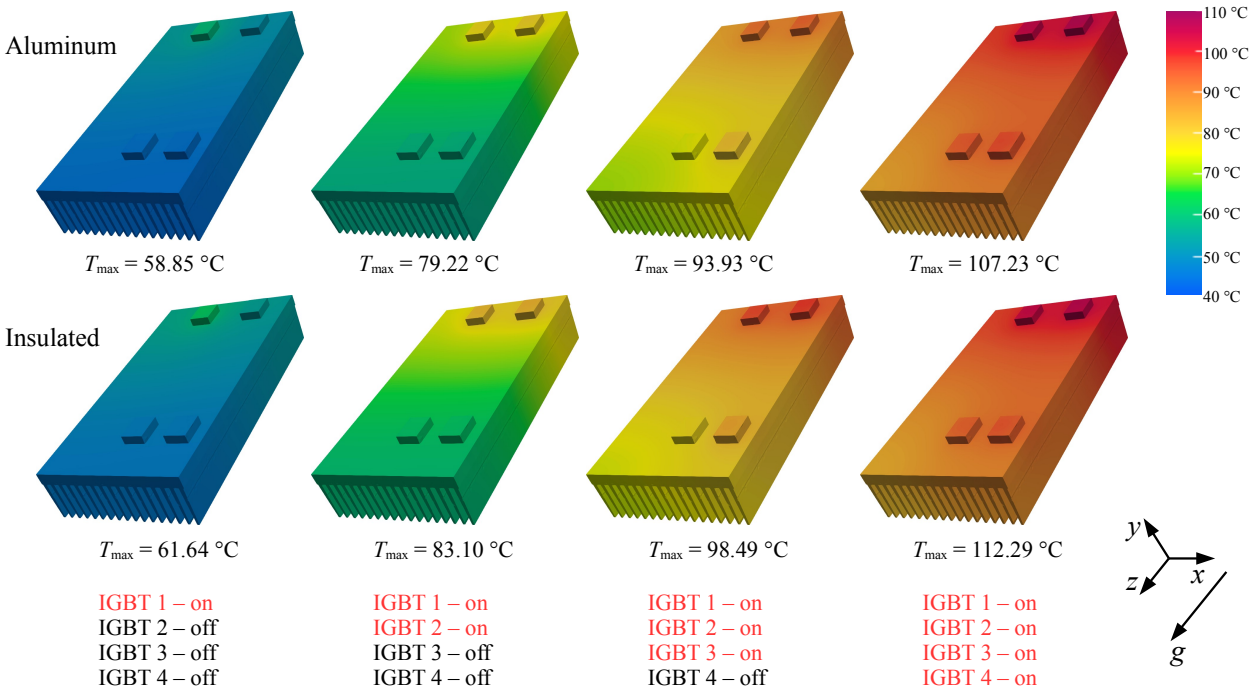

Figure 6. Temperature fields for the fins and IGBTs.

4. CONCLUSIONS

In this work, a 3D computational fluid dynamics analysis of a hybrid photovoltaic inverter has been performed. The study considered the major equipment with a detailed discretization of the geometry. Only natural convection was considered and a thermal analysis of 8 different load conditions was carried out. It was investigated the effect of these load conditions to the maximum and average temperature fields inside the inverter. Results have shown that using only natural convection to cool down the system, it is possible to have up to two heat sources (IGBTs) simultaneous on. With more than two IGBTs on, temperatures will be higher than 80 °C, what is not recommended for this type of electronic devices. In this case, it would be recommended to use forced convection by adding fans to the inverter inlets.

The use of insulated or aluminum external inverter walls was also investigated for an indoor application. In this case, it was observed that maximum equipment temperatures increase about 5 °C when the most restrictive insulated condition was assumed. Thus, for all studied cases in this word, external walls material was not a critical parameter to be considered.

Final analysis was related to the temperature distribution along the circuit board. With current electronic equipment distribution, top right corner was the region with higher temperature (close to the inverter outlets). The region with lower temperature was next to the bottom left corner (close to the inverter inlets).

5. ACKNOWLEDGMENTS

The author Jeferson A. Souza thanks CNPq – Conselho Nacional de Desenvolvimento Científico e Tecnológico for research grant (Processes: 304699/2019-5). The authors Otávio D. A. Heckler, Marcus V. A. Pereira, Rafael and Christiano Annunziato thanks the NHS - Sistemas Eletrônicos Ltda. The author Welington Fernando Lima Desan thanks Radek Sistemas de Informação Ltda, for the financial support.

6. REFERENCES

Bejan, A., 1993, “Heat Transfer”, *John Wiley & Sons*, 1sted.

Figueiredo, G., Mares, F.M., Manito, A.A., Torres, P.F. and Macêdo, W.N., 2021, “Mathematical Modeling and Computational Tool That Consider the Thermal Behavior of Inverters in the Forecast of Energy Yield in Grid-Connected Photovoltaic Systems”, *Journal of Solar Energy Engineering*, Vol. 143, No. 5, p. 051005.

Jeykishan Kumar, K., Sudhir Kumar, R. and Bhattacharjee, T., 2021, “Alternate method for evaluating power-temperature derating characteristics of grid tie solar photovoltaic inverter”, *Sādhanā*, Vol. 46, No. 3, p. 117.

Rampinelli, G.A., Krenzinger, A. and Bühler, A.J., 2017, “Methodology for Analysis of Thermal Behavior of Inverters for Photovoltaic Systems”, *Journal of Solar Energy Engineering*, Vol. 139, No. 2, p. 025501.

Roberts, J.J., Mendiburu Zevallos, A.A. and Cassula, A.M., 2017, “Assessment of photovoltaic performance models for system simulation”, *Renewable and Sustainable Energy Reviews*, Vol. 72, pp. 1104–1123.

Tan, L., Liu, P., She, C., Xu, P., Yan, L. and Quan, H., 2022, “Heat Dissipation Characteristics of IGBT Module Based on Flow-Solid Coupling”, *Micromachines*, Vol. 13, No. 4, p. 554.

Versteeg, H. and Malalasekra, M., 2007, “An Introduction to Computational Fluid Dynamics: The Finite Volume Method”, *Prentice Hall*, 2nded.

Weller, H., Greenshields, C. and de Rouvray, C. (n.d.). “The OpenFOAM Foundation Ltd”, *OpenFOAM*, available at: https://openfoam.org/.

7. RESPONSIBILITY NOTICE

The authors are the only responsible for the printed material included in this paper.